Contributions of Indian Ocean Sea Surface Temperatures to Enhanced East African Rainfall

CAROLINE C. UMMENHOFER, ALEXANDER SEN GUPTA, AND MATTHEW H. ENGLAND

Climate Change Research Centre, University of New South Wales, Sydney, New South Wales, Australia

CHRIS J. C. REASON

Department of Oceanography, University of Cape Town, Rondebosch, Cape Town, South Africa

ABSTRACT

Links between extreme wet conditions over East Africa and Indian Ocean sea surface temperatures (SST) are investigated during the core of the so-called short rain season in October–November. During periods of enhanced East African rainfall, Indian Ocean SST anomalies reminiscent of a tropical Indian Ocean dipole (IOD) event are observed. Ensemble simulations with an atmospheric general circulation model are used to understand the relative effect of local and large-scale Indian Ocean SST anomalies on above-average East African precipitation. The importance of the various tropical and subtropical IOD SST poles, both individually and in combination, is quantified. In the simulations, enhanced East African "short rains" are predominantly driven by the local warm SST anomalies in the western equatorial Indian Ocean, while the eastern cold pole of the tropical IOD is of lesser importance. The changed East African rainfall distribution can be explained by a reorganization of the atmospheric circulation induced by the SST anomalies. A reduction in sea level pressure over the western half of the Indian Ocean and converging wind anomalies over East Africa lead to moisture convergence and increased convective activity over the region. The pattern of large-scale circulation changes over the tropical Indian Ocean and adjacent landmasses is consistent with an anomalous strengthening of the Walker cell. The seasonal cycle of various indices related to the SST and the atmospheric circulation in the equatorial Indian Ocean are examined to assess their potential usefulness for seasonal forecasting.

1. Introduction

Much of the African continent faces frequent and devastating climate extremes with far-reaching economic and social consequences. These extremes are mainly related to a lack or an excess of rainfall over wide regions, often affecting the livelihood of millions, with a profound impact on rain-fed agriculture and pastoralism (Verdin et al. 2005), water and food security (Funk et al. 2005; Verdin et al. 2005), and public health (Epstein 1999). Over the past few decades, such events that caused havoc across wide parts of Africa included the devastating droughts of the 1960s to the 1980s in the Sahel region (e.g., Giannini et al. 2003), the drought-associated famine in Ethiopia in 1984/85 (Broad and Agrawala 2000), and the disastrous floods in East Africa in 1961, 1994, and 1997 (e.g., Birkett et al. 1999). Across the Horn of Africa, Linthicum et al. (1999) and Epstein (1999) directly link tens of thousands of new cases of Rift Valley fever, cholera, and malaria in 1998 to periods of heavy rainfall in late 1997 and the ensuing expansion of mosquito-prone habitats. Improved forecasts through a better understanding of the mechanisms in the climate system responsible for above-average rainfall in the region could reduce the severity of such outbreaks and ameliorate human suffering: a 2–5-month lead time would be sufficient for preventive measures such as vaccinating domestic animals and pretreating mosquito habitats with insecticides (Linthicum et al. 1999).

Several studies have focused on a particular extreme event in an attempt to understand the mechanisms involved for that specific case: for example, recent El Niño events in southern Africa (Reason and Jagadheesha

Corresponding author address: Caroline Ummenhofer, Climate Change Research Centre, University of New South Wales, Sydney, NSW 2052, Australia.
E-mail: c.ummenhofer@unsw.edu.au

2005; Lyon and Mason 2007); and for East Africa, the drought in 2005 (Hastenrath et al. 2007) and floods in 1994 (Behera et al. 1999) and 1997 (Birkett et al. 1999; Latif et al. 1999; Webster et al. 1999). Over East Africa, previous studies present clear evidence of the importance of the tropical Indian Ocean in modulating rainfall variability in observations (e.g., Black et al. 2003; Clark et al. 2003) and in climate model simulations (e.g., Goddard and Graham 1999; Latif et al. 1999). Sea surface temperature (SST) patterns associated with the zonal mode of variability, the Indian Ocean Dipole (IOD; Saji et al. 1999; Webster et al. 1999), and associated changes in the basinwide atmospheric circulation are implicated in several flooding events (e.g., Behera et al. 1999; Latif et al. 1999; Black et al. 2003; Hastenrath 2007). However, the question of which particular region(s) of anomalous SST, with coincident atmospheric circulation changes, is sufficient to induce rainfall changes over East Africa has yet to be considered. In this study, we use ensemble experiments with an atmospheric general circulation model (AGCM) to quantify the contribution of SST anomalies (associated with a characteristic Indian Ocean dipole pattern discussed in previous studies) to extreme wet conditions over East Africa.

Precipitation across the African continent is highly variable in its temporal and spatial distribution. It is modulated by a multitude of factors. Of major importance are oceanic influences that include local forcing by SST in the adjacent Atlantic and Indian Oceans, as well as remote teleconnections from the tropical Pacific (e.g., Giannini et al. 2003). The atmospheric circulation is characterized by the annual progression of the Intertropical Convergence Zone (ITCZ), the seasonally varying monsoon winds, and extratropical influences to the south (e.g., Reason and Rouault 2005). The interactions between these components and the continent's many orographic features make for complex dynamics controlling African rainfall (Janowiak 1988). The present study focuses on precipitation in equatorial East Africa, a region dominated by the migration of the ITCZ and the monsoon circulation. The rainy seasons in East Africa occur during the transitions between winter and summer monsoons, when airflow from both hemispheres converges near the equator (Hastenrath 2007). The timing of the rains associated with the ITCZ lags the migration of the sun by approximately one month (Black et al. 2003). The so-called "long rains" bring several weeks of heavy rainfall during March–May associated with the relatively slow northward movement of the ITCZ. In contrast, during the core of the "short rains" in October and November, the southward migration of the ITCZ is more rapid (Black et al. 2003)

and precipitation is particularly variable (Hastenrath 2007).

Interannual variations in East African rainfall have been linked to variability in both the Indian (Goddard and Graham 1999; Latif et al. 1999; Webster et al. 1999; Black et al. 2003; Clark et al. 2003; Hastenrath 2007) and Pacific Oceans (Janowiak 1988; Mutai et al. 1998; Reason et al. 2000; Clark et al. 2003). In empirical orthogonal function (EOF) analyses of rainfall observations for the period 1979–2001, Bowden and Semazzi (2007) show the leading mode of variability in October–December (OND) East African rainfall to be associated with El Niño–Southern Oscillation (ENSO)–IOD covariability. During El Niño events, Janowiak (1988) finds rainfall in eastern Africa, east of 20°E, to be increased (decreased) by 10%–25% for the region 10°S–0° (15°–30°S). Ogallo (1988) further explores links between ENSO and seasonal East African rainfall and finds strongest correlations during the latter half of the year. For precipitation in northern Tanzania, Kijazi and Reason (2005) link wet (dry) conditions during the OND season to El Niño (La Niña) events, and to enhanced (reduced) convection and easterly (westerly) anomalies over the western equatorial Indian Ocean. However, several studies have proposed that the relationship between East African rainfall and ENSO is actually more the result of an indirect forcing by ENSO on the Indian Ocean (e.g., Goddard and Graham 1999; Latif et al. 1999; Black et al. 2003). A close coupling between the tropical Pacific and Indian Oceans during an ENSO cycle allows anomalies from the Pacific to modulate Indian Ocean variability via changes to the atmospheric Walker circulation (Black et al. 2003) and in the ocean via the Indonesian Throughflow (Meyers 1996).

The impact of the Indian Ocean is much more immediate in its influence on East African rainfall. During the core of the short rain season, rainfall in East Africa seems to be closely linked to the strength of the Wyrtki jet in the upper tropical Indian Ocean, driven by the surface westerly winds, which reinforce the westward oceanic temperature gradient and form part of the equatorial zonal–vertical circulation cell (Hastenrath 2007). Hastenrath (2007) links an uncharacteristic weakening of the westerlies over the central Indian Ocean with floods in 1961, 1994, and 1997 over East Africa. For 1994, Behera et al. (1999) report unusual conditions in the ocean–atmosphere system of the tropical Indian Ocean, with cold (warm) SST anomalies in the eastern (western) Indian Ocean and anomalous moisture transport across the Indian Ocean region. Black et al. (2003) find years with enhanced short rains in East Africa linked to Indian Ocean SST anomalies

reminiscent of the IOD. This association is nonlinear, however: only extreme IOD years with persistent changes in the SST pattern and a concurrent easterly anomaly in the surface zonal wind field show a robust relationship with excessive East African short rains. The easterly anomalies in surface winds reduce the normal moisture transport away from East Africa; similarly shown for Tanzania by Mapande and Reason (2005a,b). Black et al. (2003) further propose that remote forcing from the Pacific associated with ENSO can predispose the Indian Ocean to an IOD event. Coupled ocean–atmosphere processes between the tropical Pacific and Indian Ocean as part of the tropospheric biennial oscillation and with effects on the Asian–Australian monsoon are explored by Meehl et al. (2003). Feng and Meyers (2003) associate both local winds and remote forcing with the formation of the eastern pole of the IOD. Similarly, Wijffels and Meyers (2004) find that surface winds from both the Pacific and Indian Ocean act to modulate the depth of the thermocline in the eastern Indian Ocean. Both upwelling-favorable easterly winds and a shallow thermocline in the Java–Sumatra region play an essential role in the formation phase of the IOD (Meyers et al. 2007). These indirect effects from the Pacific via the Indian Ocean could thus result in the statistical relationship between East African rainfall and ENSO described in earlier studies (cf. Janowiak 1988; Ogallo 1988).

Goddard and Graham (1999) use AGCM experiments to assess the relative contribution of the Indian and Pacific Ocean to East African rainfall variability. They force an AGCM with realistic SST variability in the Indian and Pacific Oceans separately and then compare results to a simulation with realistic SST variability globally. In the Indian Ocean simulations, convergent westerly (divergent easterly) flow results from warm (cool) SST anomalies in the western tropical Indian Ocean enhancing (reducing) moisture flux over central East Africa. Increased rainfall over East Africa occurs because of enhanced convective heating causing anomalous cyclonic circulation conditions to the southeast of Africa with southeasterly moisture flux onto East Africa (Goddard and Graham 1999). The influence of the Indian Ocean can be modulated by remote forcing from the central and eastern tropical Pacific Ocean with warm (cool) Pacific SST associated with anomalous eastward (westward) surface zonal winds and downward (upward) vertical motion over equatorial Africa and the tropical Indian Ocean. This situation increases (reduces) convection over the African tropics and the western Indian Ocean, shifting the ITCZ poleward (equatorward; Goddard and Graham 1999). Latif et al. (1999) find similar results in their AGCM simulations

forced with 1997/98 SST patterns in the Indian and Pacific Ocean separately to explain the excessive rainfall in East Africa during that period. The anomalous Indian Ocean SST of 1997/98 with unusually warm (cold) SST in the western tropical Indian Ocean is sufficient to induce the observed East African rainfall changes. In contrast, Pacific Ocean SST is not directly responsible for the increased rainfall over East Africa. However, as previously discussed, there are indications that the unusual Indian Ocean SST patterns at the time were remotely forced by the Pacific Ocean via anomalous surface heat fluxes (Latif et al. 1999). Black et al. (2003) propose that the indirect ENSO–East African rainfall relationship via modulation of the tropical Indian Ocean can explain interdecadal variations in East African rainfall, with both ENSO and the IOD suppressed during the mid-1940s to the early 1960s. They further hypothesize that improved long-term predictability of East African rainfall could be gained from an understanding of ENSO's influence on tropical Indian Ocean dynamics.

Rocha and Simmonds (1997a) find both the Southern Oscillation index (SOI) and an index focused on pressure differences across the Indian Ocean to be potential predictors of austral summer rainfall over southeastern Africa, best used in conjunction as they are largely independent. Mutai et al. (1998) use rotated EOF analysis of global SST anomalies to predict interannual variability in the East African short rains for the OND season. They find the dominant SST modes to be associated with large-scale changes in the tropical atmospheric circulation with anomalies in the near-surface divergence/convergence over the three ocean basins and ultimately with continental African rainfall. Strong correlations between these SST modes and East African rainfall are evident at zero lag; however, only one of the EOF predictors promised any predictive skill at longer lead times (Mutai et al. 1998). In contrast, Hastenrath et al. (2004) investigate the skill of atmospheric circulation indexes over the tropical Indian Ocean region to help with forecasts of the East African short rains. This approach attempts to exploit the tight relationship between equatorial surface westerlies over the Indian Ocean and the coastal East African short rains (Hastenrath et al. 1993). However, as the Indian Ocean boreal autumn zonal circulation cell, despite its intensity, develops very rapidly without any long-lived precursors, the predictive potential gained from any circulation indices is very limited (Hastenrath et al. 2004). In this study, we aim to gain a better understanding of the influence of local Indian Ocean SST on the regional atmospheric circulation. This would help in pinpointing more long-lived oceanic precursors that predispose the Indian Ocean to

TABLE 1. Summary of observation- and reanalysis-based precipitation products used and the period analyzed in this study.

Product	Description	Period	Reference
NNR	Reanalysis data product from the NCEP–NCAR reanalysis. Precipitation is not constrained by observations, but derived completely from model 6-h forecasts.	1979–2006	Kalnay et al. (1996); Kistler et al. (2001)
CAMSOPI	National Oceanic and Atmospheric Administration (NOAA) NCEP Climate Prediction Center (CPC) Climate Anomaly Monitoring System–OLR Precipitation Index. Merged analysis product that combines rain gauge data with satellite-derived OLR Precipitation Index estimates.	1979–2006	Janowiak and Xie (1999)
GPCC	Global Precipitation Climatology Centre (GPCC) product. Incorporates global data from 10 000–43 000 stations, depending on the time coverage.	1979–2004	Fuchs et al. (2007)
CMAP	CPC Merged Analysis of Precipitation (CMAP) product. Combines several diverse datasets, including gauge-based analyses from GPCC, predictions by the operational forecast model of European Centre for Medium-Range Weather Forecasting (ECMWF), and three types of satellite estimates.	1979–2006	Xie and Arkin (1996)

extreme situations, as occurred in 1961, 1994, and 1997 with excessive short rains over East Africa. Even a two-month lead time, which is not unrealistic with oceanic precursors, could allow preventive measures to greatly reduce the economic and social impacts over East Africa (Linthicum et al. 1999).

Interestingly, Hastenrath et al. (2004) and Hastenrath (2007) report a decline in the strength of the relationship between the equatorial zonal circulation and the East African short rains over the period 1978–96 relative to the earlier period 1958–77, despite the zonal equatorial circulation cell retaining its previous strength. Landman and Mason (1999) also describe a weakening of the ENSO signal in Indian Ocean temperatures since the late 1970s. As a result, relationships between tropical Indian Ocean variability and summer rainfall over South Africa and Namibia may have changed, with warm (cold) SST anomalies in the western tropical Indian Ocean associated with wet (dry) conditions over northeastern South Africa and Namibia over the last few decades (Landman and Mason 1999). In light of these findings, a better understanding of the factors contributing to enhanced East African rainfall is essential. The overarching goal of the present study is to explore the contributions of local and large-scale SST to enhanced East African short rains via changes of the atmospheric circulation across the Indian Ocean.

The remainder of the paper is structured as follows: section 2 describes the datasets (observational and reanalysis), the climate model and the model experiments used in the study. In section 3, observed and model rainfall characteristics are described over the African continent and locally for the East African region. The observed SST anomalies associated with extremes in the East Africa short rains are explored in section 4 and related to the SST anomalies used in the model simulations. Section 5 presents the changes in the atmospheric circulation in the

model simulations and a mechanism for the induced shifts in the rainfall distribution is proposed. The main results are summarized in section 6.

2. Datasets and climate model

a. Observational and reanalysis data

A suite of observation- and reanalysis-based precipitation products are used to assess the model's representation of precipitation over the African continent and the Indian Ocean region. Monthly precipitation data for the post-1979 period is taken from several products, when these products generally become more reliable. All products are provided at a 2.5° latitude–longitude resolution. Brief details are given in Table 1.

b. Climate model

The climate model used for the experiments is the National Center for Atmospheric Research (NCAR) Community Climate System Model, version 3 (CCSM3; Collins et al. 2006), run in the atmosphere-only mode. The atmospheric component of CCSM3, the Community Atmosphere Model, version 3 (CAM3), uses a spectral dynamical core at a T42 horizontal resolution (approximately 2.8° latitude–longitude) and 26 vertical levels. The CCSM3 model, its components, and configurations are described in Collins et al. (2006), and more specifically the atmospheric component CAM3 by Hurrell et al. (2006). Several studies assess the model's performance and suitability for applications in climate research relevant for the present study, in particular in regard to the representation of the hydrological cycle (Hack et al. 2006), tropical Pacific climate variability (Deser et al. 2006), ENSO variability (Zelle et al. 2005), and monsoon regimes (Meehl et al. 2006). Several biases in the model have been documented: most notably

associated with tropical Pacific climate, that is, the ITCZ, South Pacific Convergence Zone (SPCZ; e.g., Zhang and Wang 2006), and ENSO spatial and temporal variability (e.g., Deser et al. 2006). These issues and their relevance for the Indian Ocean region have been explored in detail by Ummenhofer et al. (2008).

c. Experimental setup

In complementary studies, England et al. (2006) and Ummenhofer et al. (2008) investigated the link between southwest Western Australian (SWWA) precipitation and anomalous Indian Ocean SST. Ummenhofer et al. (2008) find that the frequency distribution of precipitation in this region is associated with a characteristic SST tripole pattern very similar to the dominant mode of SST variability in the Indian Ocean (defined through an EOF analysis; Santoso 2005). England et al. (2006) in observations and Ummenhofer et al. (2008) in model experiments demonstrate that, in addition to SWWA, there is also a strong link between this SST pattern and precipitation over regions including East Africa. In the present study, the perturbation experiments of Ummenhofer et al. (2008) are further analyzed, now focusing on the East African region, and additional experiments are performed in which the original perturbation pattern is broken into its regional component poles.

In the control experiment the CCSM3 in atmosphere-only mode is forced with the monthly SST climatology, which is based on Reynolds SST (Smith and Reynolds 2003, 2004) and Hadley anomalies (Rayner et al. 2003). For a more detailed description of the SST climatology see Hurrell et al. (2006). A set of 80 one-yr ensemble runs, each starting on 1 January from different initial atmospheric conditions and using this SST climatology, comprises the control experiment set (CNTRL). In the perturbation experiments, monthly varying SST anomalies are added to the standard climatology across the Indian Ocean region. The full seasonally evolving SST perturbation pattern is described in Ummenhofer et al. (2008) and features components of both a tropical IOD and a subtropical IOD (SIOD) signal. This pattern closely resembles a dominant mode of variability in the Indian Ocean (Santoso 2005) and previous work has explored certain components of these characteristic SST features in the tropical (e.g., Saji et al. 1999; Webster et al. 1999) and the subtropical Indian Ocean (e.g., Behera and Yamagata 2001; Reason 2002), as well as links between the two in the eastern Indian Ocean (e.g., Nicholls 1989; Ummenhofer et al. 2008). Additional experiments are also carried out using various regional subsets of the poles evident in the full pattern (see below). The average October–November SST anomalies used in

the perturbation runs are shown in Fig. 1. This is the season when the anomalous SST are generally the most pronounced. For reference, the detailed monthly varying SST anomalies can be seen in Fig. 1 in Ummenhofer et al. (2008). A set of 60 one-yr ensemble runs are carried out for each of the perturbation fields applied. The entire anomalous SST pattern shown in Fig. 1 over the Indian Ocean region is termed P_I. To assess the importance of local SST anomalies in modulating East African rainfall, and to quantify their separate contributions, perturbation experiments are also conducted with particular local poles of SST anomalies only: P_{eI} with the eastern tropical IOD pole only (centered at 10°S, 110°E), P_{wI} with the western tropical IOD pole only (centered at 0°, 50°E), P_{eI+wI} with the eastern and western tropical IOD poles only, the SIOD pole P_{sI} (centered at 30°S, 95°E), and P_{eI+sI} with the eastern and southern poles only. The locations of the poles used in the different experiments are indicated as dashed boxes in Fig. 1. To reduce spurious atmospheric circulation set up by unrealistic gradients at the "edges" of the poles, smoothing has been applied. For more details see section 4.

3. Observed and model rainfall characteristics

The spatial and temporal characteristics of precipitation in the model are assessed across the African region and compared to observations (Fig. 2). The observed large-scale features of annual precipitation with the arid areas across northern and southern Africa are well represented in the model (Figs. 2a,b). However, in the model, the high-rainfall region in western and central equatorial Africa receives an excess of precipitation of the order of 20%–30% compared to observations. Over tropical eastern Africa, the band of high rainfall also extends too far east into the Ethiopian highlands. In addition, the observed low-rainfall regime over the Horn of Africa is confined too close to the coast in the model. Over the equatorial Indian Ocean, the observed high-rainfall region associated with the ITCZ is split into two in a classical double-ITCZ configuration, a common problem in general circulation models (Meehl and Arblaster 1998; Hurrell et al. 2006). The excessive precipitation in the model over the Bay of Bengal is due to the fact that the tropical maximum remains north of the equator throughout the year (Hack et al. 2006; Hurrell et al. 2006). The major spatial and temporal features of the monsoonal precipitation patterns are suitably well represented by the model (Meehl et al. 2006).

Focusing on East Africa, the October–November precipitation time series as the core of the short rain season are shown spatially averaged over the region delimited by 9°N–1°S, 29°–46°E (10°N–1°S, 31°–45°E)

SST (Oct–Nov)
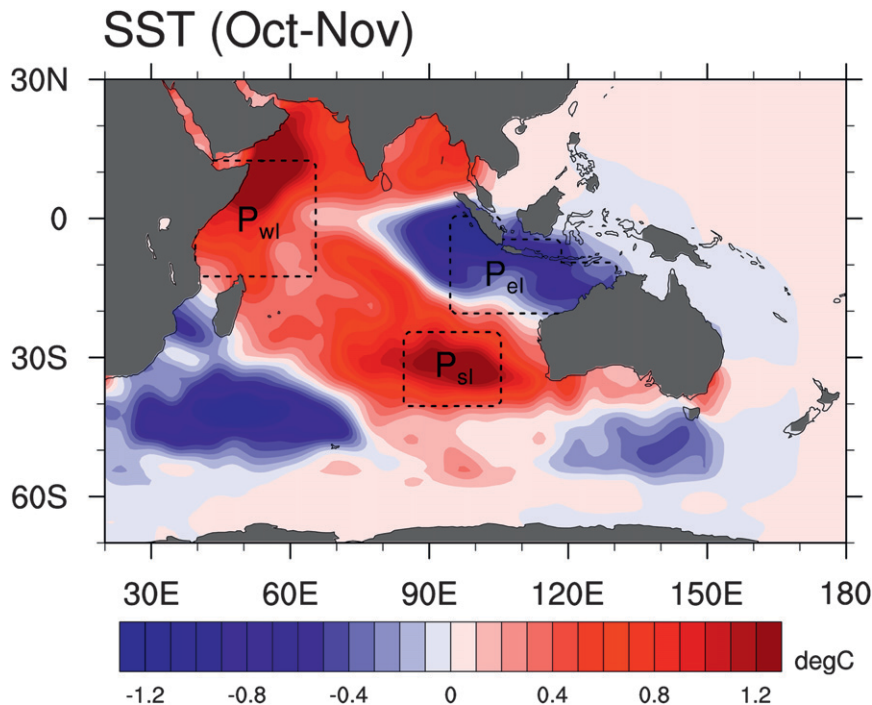
FIG. 1. Average October–November SST anomaly (°C) superimposed as a perturbation on the climatological SST across the entire Indian Ocean (P_I) and for individual poles separately, with the poles indicated by the dashed boxes as P_{wI}, P_{eI}, and P_{sI}.

for the observed (model) in Figs. 2c,d, shown as standardized anomalies for ease of comparison. The study area in the observations is chosen to match the one in the model that recorded the largest response to the SST perturbations in the simulations. For the October–November months during 1979–2006, East Africa received on average 77 mm month^{-1} with a standard deviation of 26 mm month^{-1}. The years 1983 and 1997, and to a lesser degree 2006, in the East African rainfall time series stand out as years with enhanced short rains (Fig. 2c). A pronounced long-term decline in East African rainfall is apparent when focusing on the period since 1960, with a steady drop in lake levels (Birkett et al. 1999). However, because of the sparse station data coverage over the region (e.g., Verschuren et al. 2000), we limit our comparison to the post-1979 period with good satellite estimates, and no significant [at 90% confidence level (CL)] observed rainfall trend. As mentioned previously, the simulated East African rainfall is substantially higher at 187 mm month^{-1} and with a standard deviation of 19 mm month^{-1}. However, with a direct comparison of the model and observed rainfall time series, one has to be mindful that the model is forced with SST climatology, which could account for the damped variability. For the same length of record, the standardized anomalies of East African precipita-

tion in the model show, as in the observed, two years with enhanced short rains above 2 standard deviations month^{-1} (Fig. 2d). However, negative excursions with rainfall below 1 standard deviation are more common in the model than in the observed (Figs. 2c,d).

The seasonal cycle of East African rainfall exhibits distinct maxima in the March–May and October–November months, representing the core months of the "long" and "short" rains, respectively (e.g., Black et al. 2003). The modeled precipitation captures the double peaked seasonal cycle (Fig. 2e), although the peaks, particularly the one associated with the short rains, are overly pronounced. Details of the model's representation of the monsoon circulation and precipitation are described by Meehl et al. (2006). The observed East African rainfall exhibits dominant periodicity at 5 and 2 yr, compared to the model 10, 6.5, 3.5, 3, and 2 yr.

4. Observed and model SST anomalies

Composites of SST during years of anomalous short rains are shown in Fig. 3. For different observation- and model-based precipitation products (details see Table 1), years with extreme conditions during the short rain season are defined as those exceeding ±1 standard deviation in the area-averaged, detrended time series of
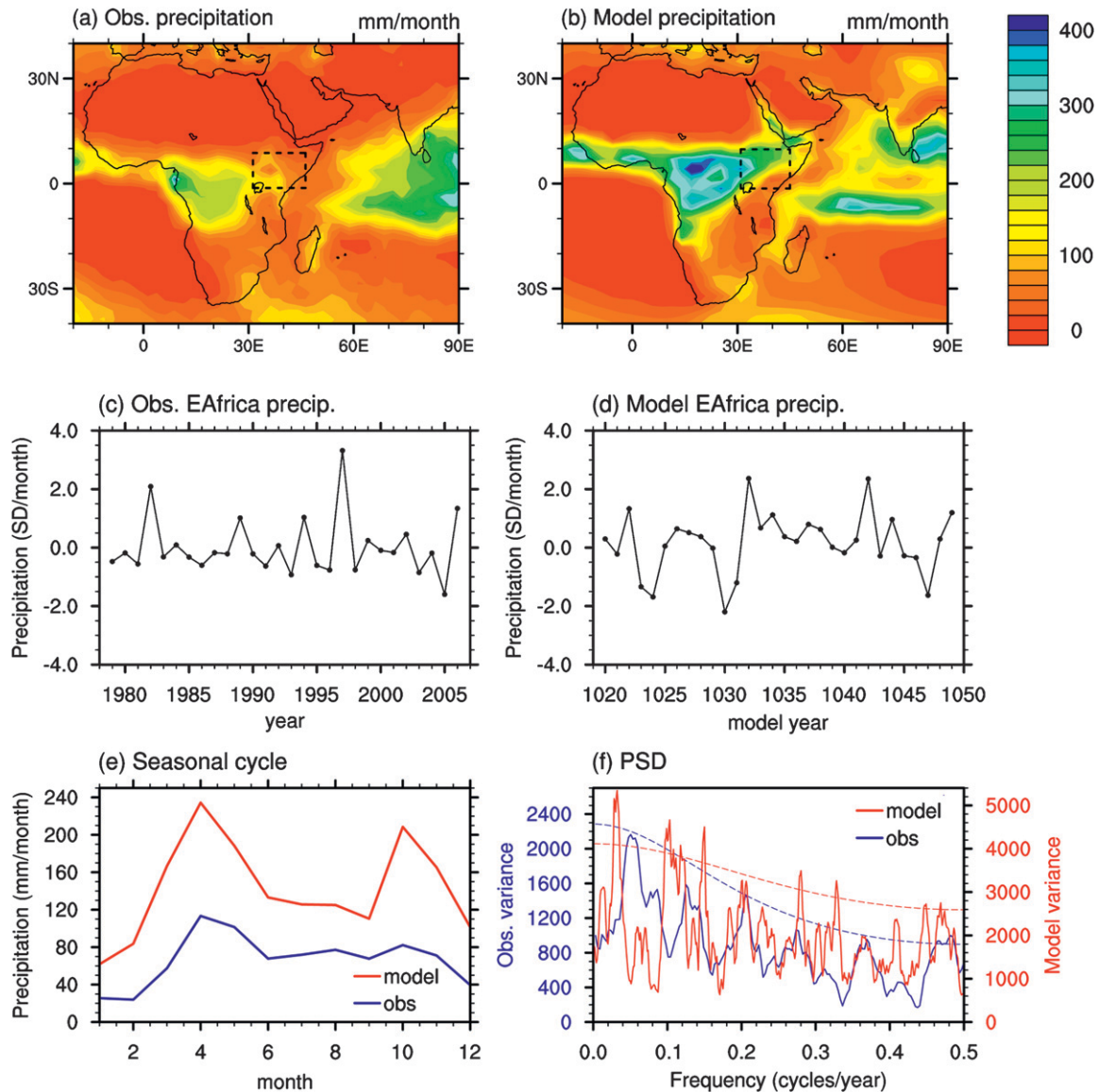
FIG. 2. October–November long-term mean of (a), (b) rainfall (mm month^{-1}) across the African continent and the Indian Ocean region with observed (model) on the left (right). The long-term mean in the observations in (a) is based on CAMSOPI data for the period 1979–2006; the model field in (b) on the 80-yr control run. The dashed boxes in (a) and (b) indicate the area used to derive (c), (d) the observed and model East Africa October–November precipitation time series shown as standardized anomalies. (e) The long-term seasonal cycle in precipitation for the observed (blue) and model (red). (f) The power spectral density shows the observed (model) variance for the dominant cycles in blue (red), with the dashed lines indicating a 95% CL according to a theoretical Markov spectrum.

East African precipitation (Figs. 3a,d,g,j). With the exception of the National Centers for Environmental Prediction (NCEP)–NCAR Reanalysis (NNR), all products show a positive trend in precipitation during the October–November season of 0.6–0.8 mm month^{-1} yr^{-1}. Two years with very excessive short rains are common to all precipitation products, namely 1983 and 1997. Extensive flooding during the latter year has inspired previous work (e.g., Birkett et al. 1999; Latif et al.

1999). In addition, 2006 recorded anomalous wet conditions during the short rain season in all products that cover that period (GPCC data are only available up to 2004). In contrast, short rain seasons with very much reduced precipitation are more variable across the products, with relatively few years qualifying as extremely dry during the short rain season. Among the years receiving very much reduced precipitation during the short rain season, 2003 and 2005 feature in most of the
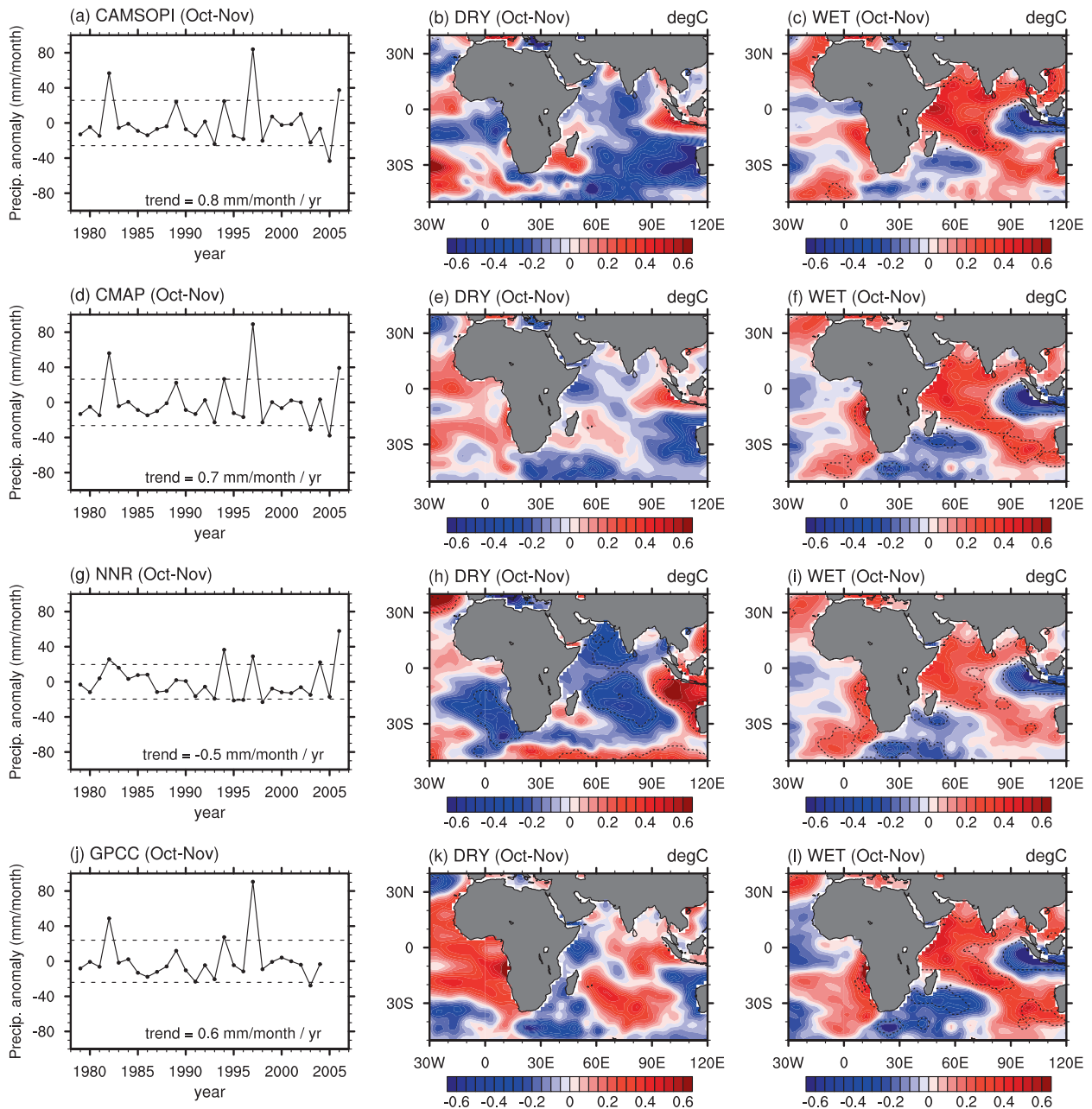
FIG. 3. (a),(d),(g),(j) Time series of East African rainfall averaged over October–November for the period 1979–2006, with ±1 std dev indicated (dashed horizontal lines). SST anomaly (°C) for the (b),(e),(h),(k) extreme dry and (c),(f),(i),(l) wet years, determined as those exceeding ±1 std dev in the respective rainfall time series. (top) to (bottom) Different precipitation products such as CAMSOPI, CMAP NNR, and GPCC, with the linear trend removed from each time series, indicated at the bottom of the left-hand panels. Dashed lines over the SST panels indicate significant anomalies at the 90% CL as estimated by a two-tailed t test.

precipitation products. The small number of years with dry conditions during the short rain season is in part due to the non-Gaussian nature of the precipitation distribution, reducing the validity of the standard deviation measure for identifying extreme years. However, the metric is successful in identifying years with wet conditions during October–November, the core of the short

rain season. Furthermore, despite small variations in the set of years chosen for the composites of SST anomalies, robust SST features across the Indian Ocean are evident for the dry and wet extremes (described below).

During short rain seasons with reduced rainfall in East Africa, the Indian Ocean is characterized by localized warm SST anomalies in the eastern Indian

Ocean off Sumatra, consistent across the different precipitation products (Figs. 3b,e,h,k). Across the remainder of the Indian Ocean during dry October–November seasons the composite patterns are less consistent, although there is a tendency toward below-average SST in the western region of the Indian Ocean. Similarly, for the 2005 drought in East Africa, Hastenrath et al. (2007) describe anomalous cold (warm) SST anomalies in the northwest (southeast) of the equatorial Indian Ocean, a steepened eastward pressure gradient, and strengthened westerlies. SST anomalies over the Atlantic show no consistent pattern across the dry composites. In contrast, during short rain seasons with anomalous wet conditions, an area of warm SST anomalies in the western Atlantic off Angola, Namibia, and South Africa is common across all the SST composites. Colberg et al. (2004) link a similar warming in the South Atlantic to changes in the trade winds and surface heat fluxes associated with El Niño. Over the Indian Ocean, October–November SST anomalies are cold off Sumatra in the tropical eastern Indian Ocean, while warm anomalies extend over much of the western half of the Indian Ocean and the subtropical region toward Australia (Figs. 3c,f,i,l). Indian Ocean SST anomalies are significant over much of the domain and the overall pattern is very robust across all the wet composites. The pattern of Indian Ocean SST anomalies closely matches those associated with heavy East African September–November (SON) precipitation for the period 1900–97 in Black et al. (2003, their Fig. 3). The magnitude of SST anomalies in Fig. 3 is larger than in Black et al. (2003), as we focus on the October–November months and a much smaller number of extreme years in the composite. So, despite the short record and sparsity of high-quality observations over the East African region, persistent features in Indian Ocean SST anomalies concurrent with excessive rainfall during the short rain season can be identified. These observed Indian Ocean SST anomalies associated with excessive East African short rain seasons are now compared to the SST forcing fields used for a set of AGCM experiments.

The model simulations with the anomalous SST perturbations across the entire Indian Ocean (P_I) are taken from experiments described in previous work by Ummenhofer et al. (2008). They use composite patterns of observed monthly SST anomalies across the Indian Ocean for extreme dry (and wet) years over SWWA (England et al. 2006; Ummenhofer et al. 2008). Ummenhofer et al. (2008) show that extreme rainfall years in SWWA are associated with a basinwide reorganization of the atmospheric circulation across the Indian Ocean in response to the anomalous SST forcing. In observations, England et al. (2006) find hints of an out-of-phase relationship between rainfall in SWWA and

East Africa, linked to the changed large-scale atmospheric circulation across the Indian Ocean region. This link is further strengthened by model experiments in the CCSM3 (Ummenhofer et al. 2008), which indicate a highly significant shift in East African rainfall intensity resulting from this SST pattern. While derived for an analysis of Australian precipitation, these SST patterns are very similar to a dominant EOF mode in Indian Ocean variability (see Santoso 2005; Ummenhofer et al. 2008), containing features characteristics of both the IOD and SIOD. As such, the present study effectively examines the links between anomalously wet conditions during the short rain season in East Africa and a characteristic mode of Indian Ocean SST variability identified in previous work by the authors. We investigate the effect of both local and large-scale Indian Ocean SST anomalies on above-average rainfall in East Africa. In addition, we attempt to quantify the respective contributions of anomalous SST in various regions and propose a mechanism for the changed rainfall distribution.

The average October–November SST anomalies used in the perturbation AGCM simulations were shown previously in Fig. 1. In addition to the SST anomalies across the entire basin, simulations with individual SST poles are conducted, with the pole locations indicated as dashed boxes in Fig. 1 (for latitude–longitude coordinates see section 2c). The October–November SST anomalies are characterized by warm (cold) temperatures in the western and central (eastern) tropical Indian Ocean (Fig. 1). An area of anomalously cold SST is located south of Madagascar. The SST pattern in Fig. 1 resembles anomalies associated with above-average rainfall in East Africa (Fig. 3; Black et al. 2003). In an AGCM, Reason (2002) investigates the impact of South Indian Ocean SST anomalies reminiscent of the forcing used here in the P_I case, that is, cold (warm) SST anomalies in the southwest Indian Ocean south of Madagascar (in the southeast Indian Ocean off the west coast of Australia), on the atmospheric circulation over southern Africa. Despite using characteristic basinwide Indian Ocean SST anomalies extending across both the tropics and the subtropics, the focus in the present study is on tropical East African rainfall. In addition, a *quantification* of the relative influence of individual (and combined) poles to excessive East African rainfall during the short rain season is attempted.

5. Changed atmospheric circulation in model experiments

a. Rainfall distribution

The simulated total precipitation during the core of the short rain season (October–November) is spatially

averaged across East Africa (subregion indicated in Fig. 2) for each of the ensemble members in the control and the perturbed cases. The rainfall frequency distribution for each of the perturbed cases with the control distribution superimposed is shown in Fig. 4. A nonparametric Mann–Whitney rank test (von Storch and Zwiers 1999) is used to determine the significance level at which the rainfall frequency distribution over East Africa in the perturbed cases differs from the control. For P_I with the SST anomalies applied over the entire Indian Ocean, the rainfall distribution over East Africa is shifted significantly (at 99% CL) relative to the CNTRL during the October–November period (Fig. 4a). In fact, the rainfall distribution for the CNTRL and P_I barely overlap, which represents an increase in mean October–November rainfall of over 35% from 410 to 560 mm. This increase in P_I seems to be predominantly driven by the SST anomalies in the local western pole: both of the other experiments that contain a perturbed western pole (i.e., P_{eI+wI} and P_{wI}) show an increase in precipitation of comparable magnitude (Figs. 4c,f). In contrast, the ensemble sets with only the eastern and/or southern pole show no significant changes in rainfall over East Africa (Figs. 4b,d,e).

The spatial distribution of the precipitation anomalies across the Indian Ocean basin are assessed in Fig. 5. Throughout the study, we use a two-tailed t test to determine the significance of the spatial anomaly fields. This test estimates the statistical significance at which the anomalies in the perturbed experiments are distinguishable from the control at each grid point. The rainfall response over East Africa in the P_I case forms a band of increased precipitation extending from the Horn of Africa to the southwest toward the Atlantic coast (Fig. 5a). Again, the enhanced rainfall over the African continent seems to be linked to the warm SST anomalies in the western Indian Ocean, as both P_{eI+wI} and P_{wI} show a similar signal (Figs. 5c,f). All three cases with warm western Indian Ocean SST also record increased precipitation overlying the area with above-normal SST. Over southeastern Africa, P_I also shows below-average rainfall. Similarly, Rocha and Simmonds (1997b) describe anomalous dry conditions over southeastern Africa linked to warm SST in the tropical Pacific and Indian Ocean in AGCM experiments. Interestingly, they find the drought conditions over southeastern Africa to be exacerbated with co-occurring cool SST in the South Indian Ocean, consistent with a stronger response in P_I than P_{wI} here (Figs. 5a,f). Over the eastern equatorial Indian Ocean, reduced precipitation occurs over the region with anomalous cold SST and the adjacent Indonesian Archipelago (Figs. 5a,b,d). These results demonstrate a strong precipitation response re-

lated to tropical SST anomalies, but no such response from the subtropical forcing (Fig. 5e).

In summary, enhanced East African rainfall during the short rain season seem to be predominantly driven by the local warm SST anomalies in the western equatorial Indian Ocean, while the eastern cold pole is of lesser importance. The mechanisms by which the different poles change the large-scale atmospheric circulation and thus contribute to changed East African rainfall will be investigated in detail below.

b. Circulation anomalies

Both the large-scale and local SST anomalies give rise to significant changes in the overlying atmosphere, modulating its thermal and circulation characteristics. An extensive area of negative sea level pressure (SLP) anomalies (in excess of 2 hPa below average) occurs over the warm western half of the Indian Ocean and the adjacent central and east African continent in the P_I case (Fig. 6a). The reduced SLP extends to the south of Africa, west across the South Atlantic, and to the north over the Arabian Peninsula, India, and central Asia. In contrast, positive SLP anomalies occur over the eastern equatorial Indian Ocean associated with the cold SST pole (Fig. 6a). The positive SLP anomalies in the eastern Indian Ocean are a consistent feature across all the perturbed cases with a cold eastern SST pole (Figs. 6a–d). In the P_{eI+wI} and P_{wI} cases, locally negative SLP anomalies are centered over the western Indian Ocean warm pole and the East African coast and also extend west to the south of Africa (Figs. 6c,f). Geostrophic theory (Gill 1982) suggests that a near-surface low (high) will be generated in response to the warm (cool) SST forcing (Fig. 6). However, the overall response in anomalous SLP seems to be primarily driven by the warm western pole. This agrees with earlier AGCM studies showing the atmosphere to be more sensitive to warm than cold SST anomalies (e.g., Reason 2002; Ummenhofer et al. 2008).

The SLP anomalies result in an adjustment of the large-scale circulation seen in anomalous surface and midlevel wind anomalies. Figure 7 depicts anomalies in surface moisture fluxes as the product of surface winds and specific humidity. From this, the strength and direction of surface winds are apparent and discussed here, while a detailed description of the moisture fluxes is deferred to the end of section 5c. Strengthened westerly airflow over central Africa and easterly onshore anomalies from the Indian Ocean interact over the coast of equatorial East Africa to produce the surface wind convergence over East Africa seen for the P_I simulation during October–November (Fig. 7a). Easterly anomalies dominate over the entire width of the equatorial Indian Ocean basin, while the westerly anomalies are confined
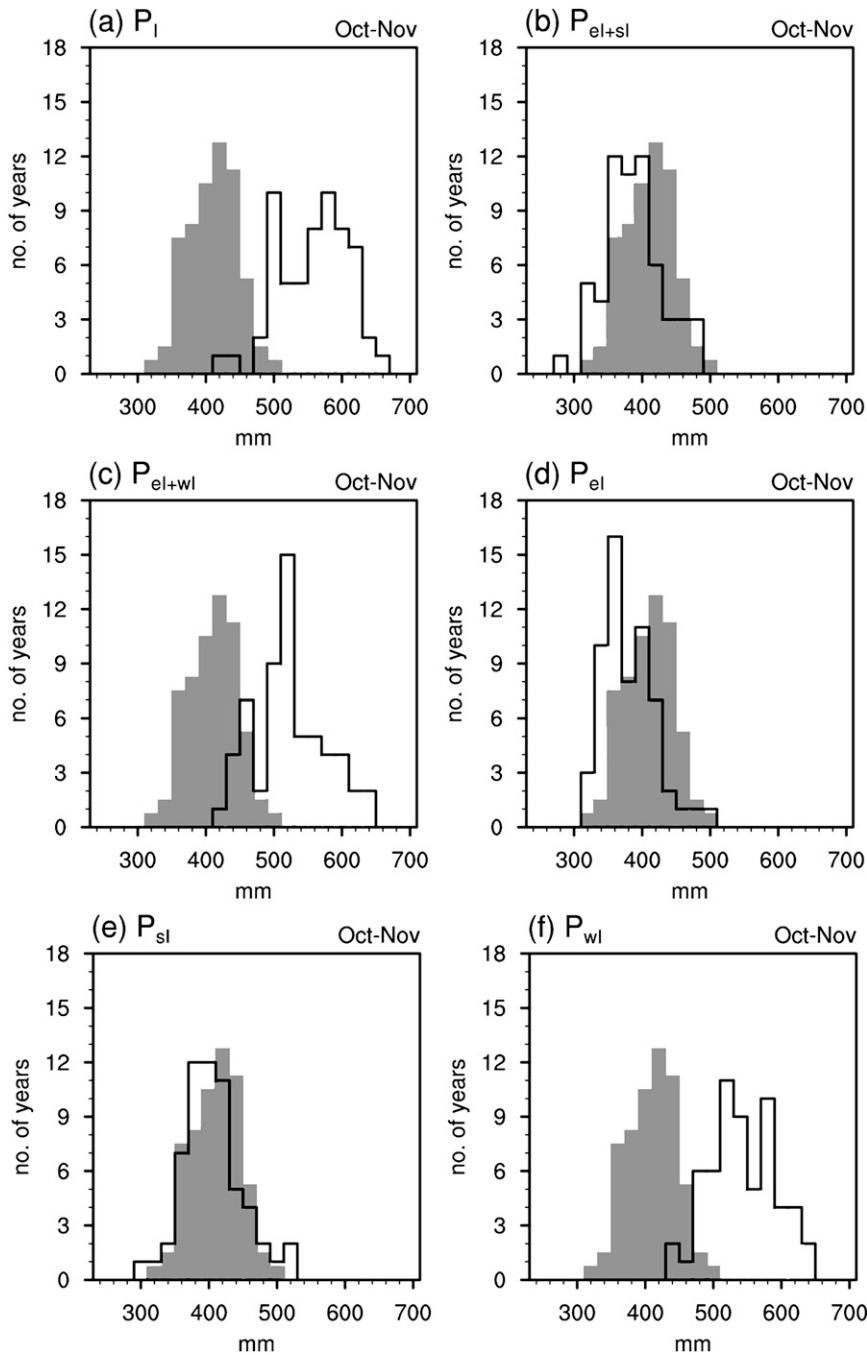
FIG. 4. Frequency distribution of total precipitation spatially averaged across East Africa (subregion indicated in Fig. 2b): rainfall amount (mm) summed for the months October–November for the following experiments: (a) P_I, (b) P_{eI+sI}, (c) P_{eI+wI}, (d) P_{eI}, (e) P_{sI}, and (f) P_{wI}. The shaded gray rainfall distribution represents the CNTRL (normalized to the number of ensemble members in the perturbed cases), while the perturbed cases are indicated with black outlines. With the exception of (e), all rainfall distributions are significantly different from the CNTRL at the 99% CL, as determined by a Mann–Whitney test.
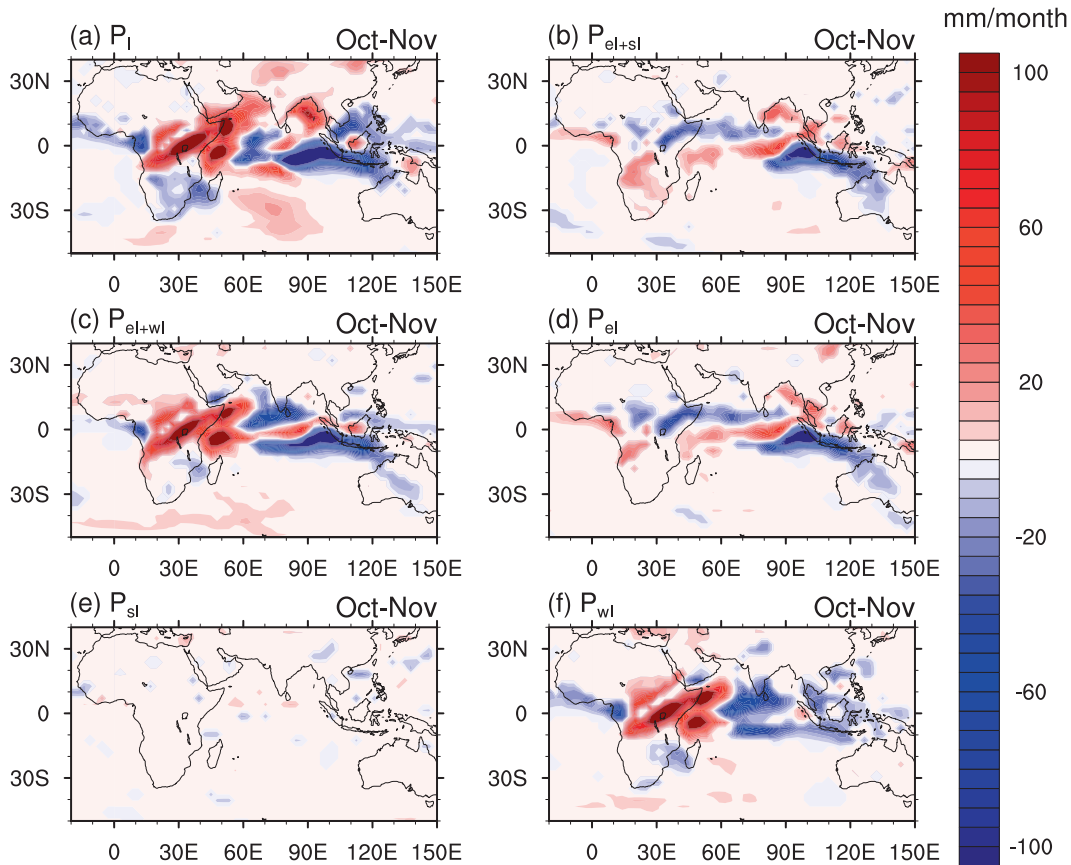
FIG. 5. Precipitation anomalies (mm month^{-1}) for (a) P_I, (b) P_{eI+sI}, (c) P_{eI+wI}, (d) P_{eI}, (e) P_{sI}, and (f) P_{wI}, averaged over the October–November months. Only anomalies are shown that are significant at the 90% CL as estimated by a two-tailed t test.

to central and eastern Africa. The western pole alone is sufficient for the local surface wind response over the East African coast, though with a more northerly component than seen in P_I (Fig. 7f). This is further confirmed in the wind anomalies at 500 hPa (figure not shown). In contrast to the surface winds, the airflow convergence at 500 hPa occurs further inland toward central Africa. Earlier studies confirm this surface-to-midlevel wind anomaly pattern associated with enhanced East African precipitation in observations (Black et al. 2003; Mapande and Reason 2005a; Hastenrath 2007) and model simulations (Goddard and Graham 1999). However, previous work tends to link these wind anomalies to the enhanced zonal pressure gradient because of the presence of both the western and eastern SST poles of the IOD. Here, we find that the wind, and thus moisture flux convergence over East Africa is predominantly driven by the local warm SST anomalies in the western equatorial Indian Ocean. The presence of the cold eastern Indian Ocean SST pole only seems to determine the extent of the zonal easterly anomalies.

The SST forcing not only affects SLP and horizontal circulation locally, but drives coherent large-scale anomalies in the basinwide zonal circulation cell. Anomalies in velocity potential are analyzed for the different experiments at the 200 hPa (Fig. 8) and at the 850-hPa level (figure not shown, as the 850 hPa results closely complement those at 200 hPa). The velocity potential represents a proxy for the strength of the zonal Walker circulation in the tropics. Anomalous out-of-phase ascent/subsidence occurs over the western/eastern Indian Ocean centered over coastal East Africa/the Indonesian Archipelago, respectively, in the P_I case (Fig. 8a). These velocity potential anomalies of opposing sign over the western and eastern Indian Ocean in the tropics and subtropics agree broadly with results by Reason (2002), though in his AGCM experiments the two poles of SST anomalies with opposite sign are imposed in the subtropical South Indian Ocean only. Low- to upper-level velocity potential anomalies of comparable magnitude are seen in the P_{eI+wI} and P_{wI} cases, though in the latter the extent of subsidence over the Indonesian
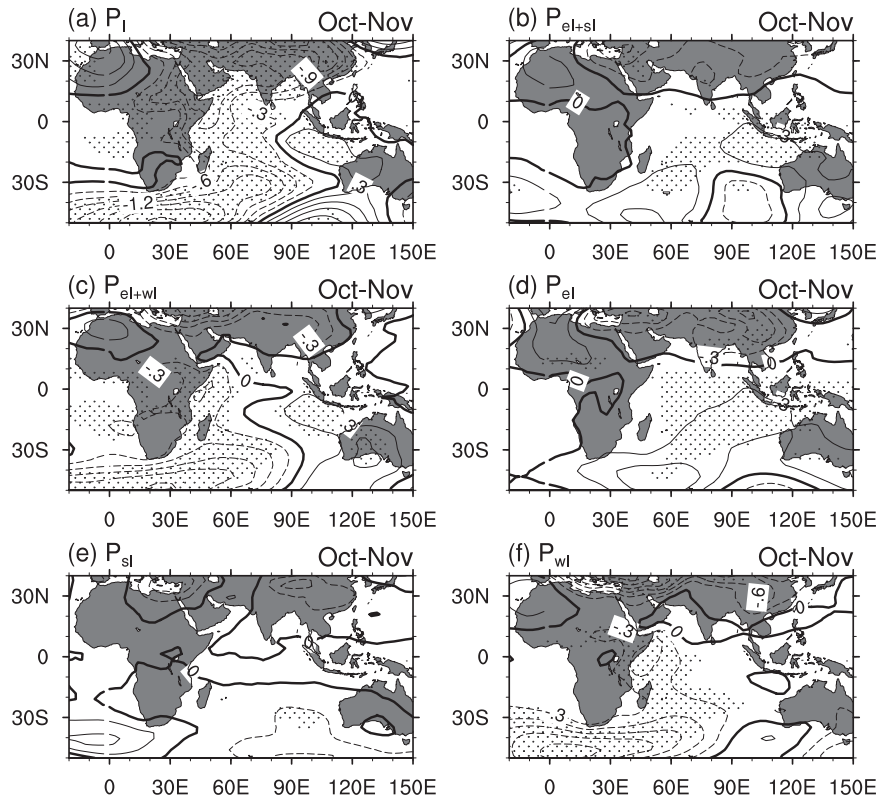
FIG. 6. SLP anomalies (hPa) for (a) P_I, (b) P_{eI+sI}, (c) P_{eI+wI}, (d) P_{eI}, (e) P_{sI}, and (f) P_{wI}, averaged over the October–November months. Stippling denotes anomalies that are significant at the 90% CL as estimated by a two-tailed t test.

Archipelago is more localized (Figs. 8c,f). This indicates that the coherent large-scale response in the Walker cell, which integrates both horizontal and vertical circulation components and to which rainfall anomalies can be linked, is due mainly to the change in the zonal SST gradient along the equator.

Anomalies in vertical velocity across the different experiments are in agreement with the circulation changes associated with the horizontal component of the Walker cell. In response to the underlying warm SST anomalies in the western equatorial Indian Ocean, changes in vertical velocity anomalies ω are recorded for P_I, P_{eI+wI}, and P_{wI} (figure not shown). Anomalous upward velocities due to enhanced convective heating occur over the western Indian Ocean and over East Africa, extending toward the southwest. The regions with upward vertical velocity anomalies closely match the areas recording increased precipitation (Figs. 5a,c,f), agreeing with earlier findings by Goddard and Graham (1999). These locally increased convective effects driven by increased buoyancy over the warm SST region are also reflected in higher penetration of the warm temperature anomalies into the atmosphere (figure not shown). In contrast, anomalous subsidence is

associated with the cold SST anomalies in the eastern equatorial Indian Ocean and the Indonesian Archipelago (figure not shown). These results agree with the anomalous strengthening of the Walker cell.

c. Thermal and moisture anomalies

To assess how much moisture is locally evaporated as opposed to advected from remote locations, anomalies in surface latent heat fluxes are shown for the different cases in Fig. 9. Positive latent heat flux anomalies in excess of 24 W m^{-2} (equivalent to approximately 0.8 mm day^{-1}) dominate over the western half of the Indian Ocean north of Madagascar and extend along the equator to 90°E in P_I (Fig. 9a). Positive anomalies of lower magnitude are seen in the subtropical Indian Ocean centered around 30°S, associated with the warm SST at the southern pole. Reduced latent heat flux anomalies of about −20 W m^{-2} (approximately −0.7 mm day^{-1}) occur in the eastern Indian Ocean for 10°N–20°S (Fig. 9a). The positive latent heat flux anomalies in the western Indian Ocean, with its associated locally evaporated moisture, potentially accounts for up to 50% of the enhanced rainfall over coastal equatorial
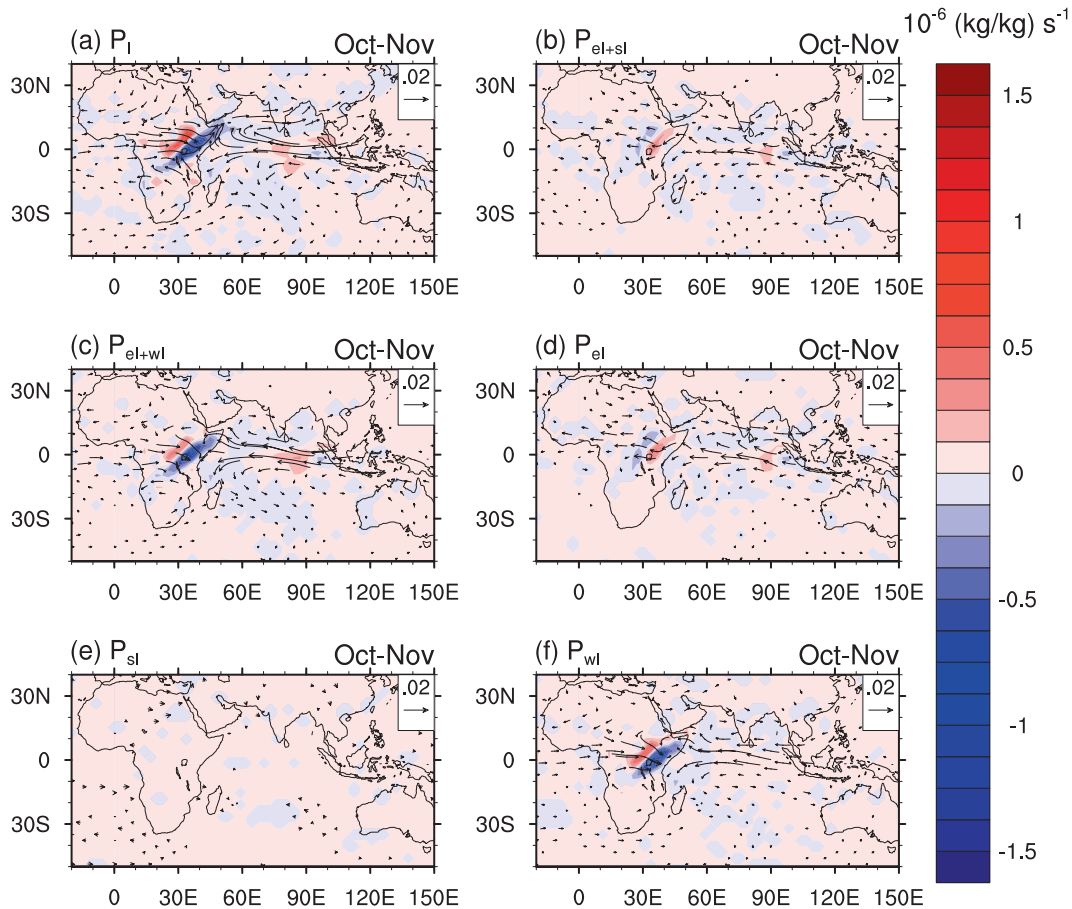
FIG. 7. Moisture flux [vectors; (kg kg^{-1}) m s^{-1}] and moisture flux divergence [colored; 10^{-6} (kg kg^{-1}) s^{-1}] anomalies at the 850-hPa level for (a) P$_I$, (b) P$_{eI+sI}$, (c) P$_{eI+wI}$, (d) P$_{eI}$, (e) P$_{sI}$, and (f) P$_{wI}$, averaged over the October–November months. Only anomalies are shown that are significant at the 90% CL as estimated by a two-tailed t test.

East Africa in the P$_I$ case (cf. Fig. 5a). In a similar way, Mapande and Reason (2005b) link enhanced rainfall in Tanzania to increased evaporation from warm SST anomalies in the adjacent ocean. Both the P$_{eI+wI}$ and P$_{wI}$ cases show the strong positive anomalies in latent heat fluxes in the western Indian Ocean, though they are more concentrated in the western basin in the latter case (Figs. 9c,f). Negative heat flux anomalies in the eastern Indian Ocean of comparable magnitude, location, and extent are seen in the P$_{eI+sI}$, P$_{eI+wI}$, and P$_{eI}$ cases (Figs. 9b,c,d). With heat flux anomalies of the order of approximately -0.7 mm day^{-1}, they can account for about 40% of the reduction in rainfall seen over the Indonesian Archipelago.

It is of further interest to explore the vertical structure of moisture anomalies induced by the anomalous SST and latent heat fluxes. Latitudinal cross sections of specific humidity anomalies centered at the equator are shown in Fig. 10 extending across the Indian Ocean basin and the adjacent continents. Following on from

previous results, only the P$_I$ and P$_{wI}$ cases are presented, as only in these cases (and in P$_{eI+wI}$; figure not shown as response is almost identical to P$_{wI}$) do distinct responses occur to the underlying SST anomaly forcing. The low-level specific humidity reflects the sign and position of the underlying SST anomalies, with positive (negative) humidity anomalies over the western (eastern) Indian Ocean (Fig. 10). The positive anomalies, which extend well into East Africa, are apparent throughout almost all of the troposphere consistent with the enhanced uplift associated with the rising branch of the Walker cell over the region. While positive specific humidity anomalies occur over the western Indian Ocean, over equatorial central and eastern Africa negative low- to midlevel humidity anomalies are evident. These seem to be directly related to the western Indian Ocean warm pole, as they remain apparent in the P$_{wI}$ case (Fig. 10b). The areas of reduced specific humidity coincide with anomalously cold air temperatures (figure not shown). The cold anomalies most likely result from reduced
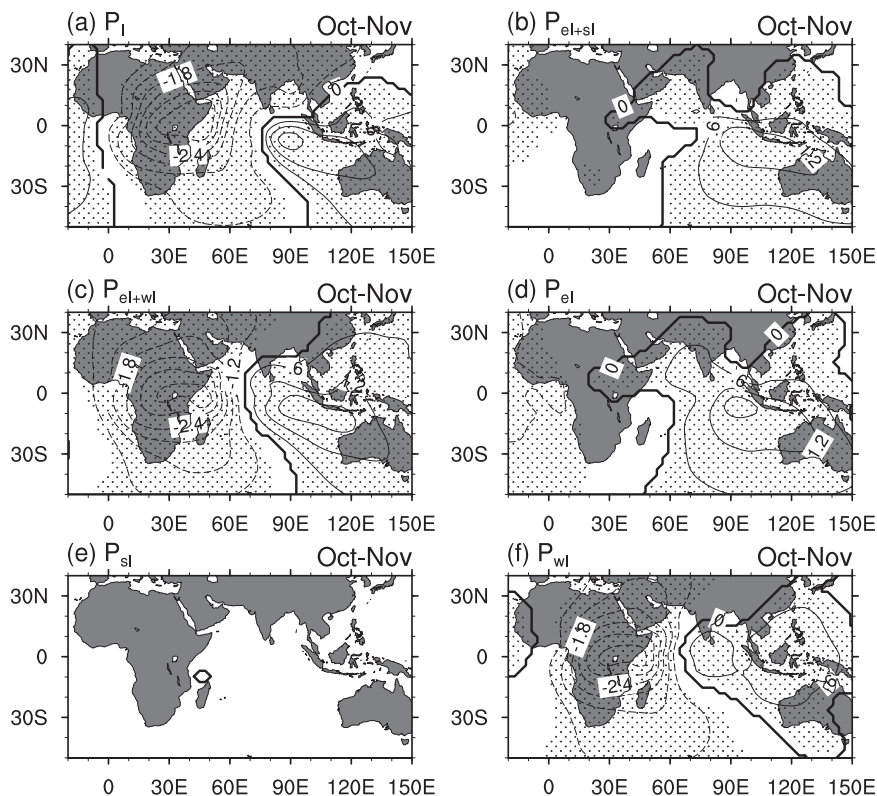
FIG. 8. Velocity potential anomalies at the 200-hPa level (10^6 m^2 s^{-1}, contour interval is 0.6 $\times$ 10^6 m^2 s^{-1}) for (a) P$_I$, (b) P$_{eI+sI}$, (c) P$_{eI+wI}$, (d) P$_{eI}$, (e) P$_{sI}$, and (f) P$_{wI}$, averaged over October–November months. Stippling denotes anomalies that are significant at the 90% CL as estimated by a two-tailed t test.

incoming solar radiation due to increased cloud cover associated with the enhanced convective activity. Mapande and Reason (2005b) find a similar reduction in observed outgoing longwave radiation (OLR), implying increased cloud cover, during anomalous wet seasons in Tanzania.

In addition to the locally derived precipitation, moisture can be advected in primarily from the ocean. Specific humidity and circulation anomalies are combined to assess changes in moisture flux, shown along with its divergence at the 850-hPa level in Fig. 7. The P$_I$ case is characterized by easterly (westerly) moisture flux anomalies along the equatorial Indian Ocean (over central equatorial Africa; Fig. 7a). Strong convergence of these anomalies occurs over much of equatorial East Africa. Similarly, Mapande and Reason (2005b) show wet years over Tanzania to be dominated by anomalous low-level moisture convergence during October, linked to warm offshore SST anomalies. In contrast over central equatorial Africa, moderate anomalous divergence in the moisture flux field is seen (Fig. 7a). This pattern of moisture flux anomalies and its convergence/divergence is reminiscent of that described by Goddard and Graham

(1999) and here also appears of comparable magnitude in the P$_{eI+wI}$ and P$_{wI}$ cases (Figs. 7c,f), while the anomalies in the other cases are very weak, or in the case of P$_{eI}$ of opposite sign. Again, this illustrates the predominant role of the western Indian Ocean warm pool in driving rainfall changes over East Africa via modulations to the local and large-scale atmospheric circulation.

d. Seasonal development of Indian Ocean anomalies

While we have thus far focused on the October–November climate response to the yearlong forced SST perturbations, it is of interest to assess their seasonal development. To better understand the atmospheric circulation response to the evolving SST anomalies, we investigate here the seasonal development of indices characterizing the state of the equatorial Indian Ocean zonal circulation. The indices, representing an averaged zonal pressure difference and the zonal surface wind, are adapted from Hastenrath (2007). Details of the calculation of these indices are provided below. Shown first in Fig. 11a are the SST anomalies for the perturbation simulations relative to the CNTRL. In general,
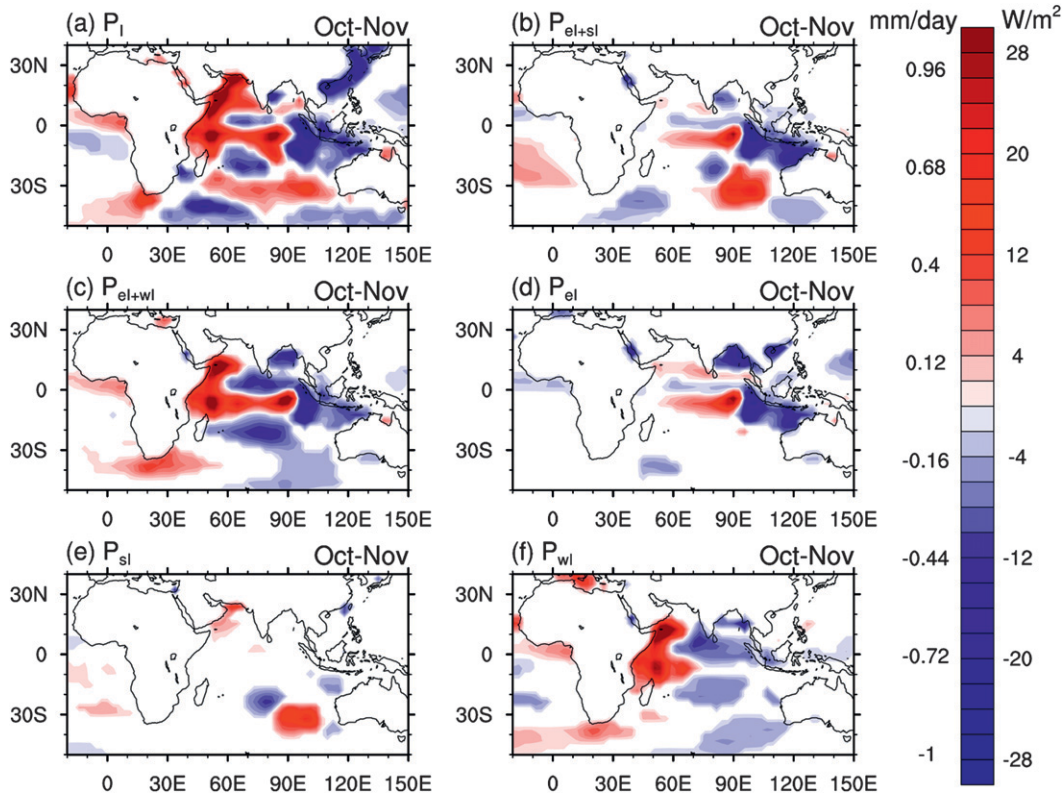
FIG. 9. Surface latent heat flux anomalies (mm day^{-1} and W m^{-2}) for (a) P_I, (b) P_{eI+sI}, (c) P_{eI+wI}, (d) P_{eI}, (e) P_{sI}, and (f) P_{wI}, averaged over the October–November months. Only anomalies are shown that are significant at the 90% CL as estimated by a two-tailed t test, with anomalies over the land either being insignificant or below the contouring interval.

the spatially averaged SST anomalies for the various poles used in the perturbation experiments are small until April, after which they increase in magnitude (Fig. 11a). Negative SST anomalies develop gradually at the cold eastern pole (P_{eI}) from May onwards, reaching a minimum value of around −0.4°C in October, after which time the anomaly rapidly decays. This is consistent with earlier findings for the seasonal evolution of the IOD (e.g., Saji et al. 1999; Webster et al. 1999; Li et al. 2003; Meyers et al. 2007). Increasingly warm anomalies occur at the western and southern poles, with a maximum of around 0.4°C for the western pole in October, while the temperatures at the southern pole continue to rise to reach around 0.5°C above normal in December. The zonal (meridional) gradient in SST anomalies; that is, the difference of SST anomalies between the western and eastern (southern and eastern) pole are also indicated in Fig. 11a as dashed lines. Both the zonal and meridional gradient in SST anomalies increases from April onwards and reach a maximum in October.

The zonal SLP gradient (pressure over the western Indian Ocean minus pressure in the east for the latitude band 7°N–7°S; SLP$_{W-E}$) determines the strength of the

zonal circulation anomalies in the equatorial Indian Ocean (Hastenrath 2007). The annual cycle of SLP$_{W-E}$ is characterized by a maximum in June–August (JJA) because of an inverse relationship between the pressure in the west and the east of the Indian Ocean, declining to a minimum in austral summer (Fig. 3c in Hastenrath 2007). For the P_I experiment, a drop relative to the CNTRL occurs in SLP$_{W-E}$ between April and May, followed by a steeper decrease from July to a minimum in October (Fig. 11b). This represents an intensification of the seasonal decrease in SLP$_{W-E}$ after August. The magnitude and seasonal evolution of this pressure difference anomaly in P_I is reproduced most closely by the P_{eI+wI} case, although the full perturbation values are slightly higher. The pressure difference is mostly due to the negative anomalies at the western pole (P_{wI} in Fig. 11b; see also Fig. 6f), while the contributions of the eastern pole (P_{eI} in Fig. 11b) are minimal. The zonal pressure difference SLP$_{W-E}$ is instrumental in driving the zonal surface wind component along the equator (U_{EQ}), measured for the latitude band 4°N–4°S (Fig. 11c). The seasonal progression of U_{EQ} shows peaks with zonal mean westerly winds of almost 3 m s^{-1} during
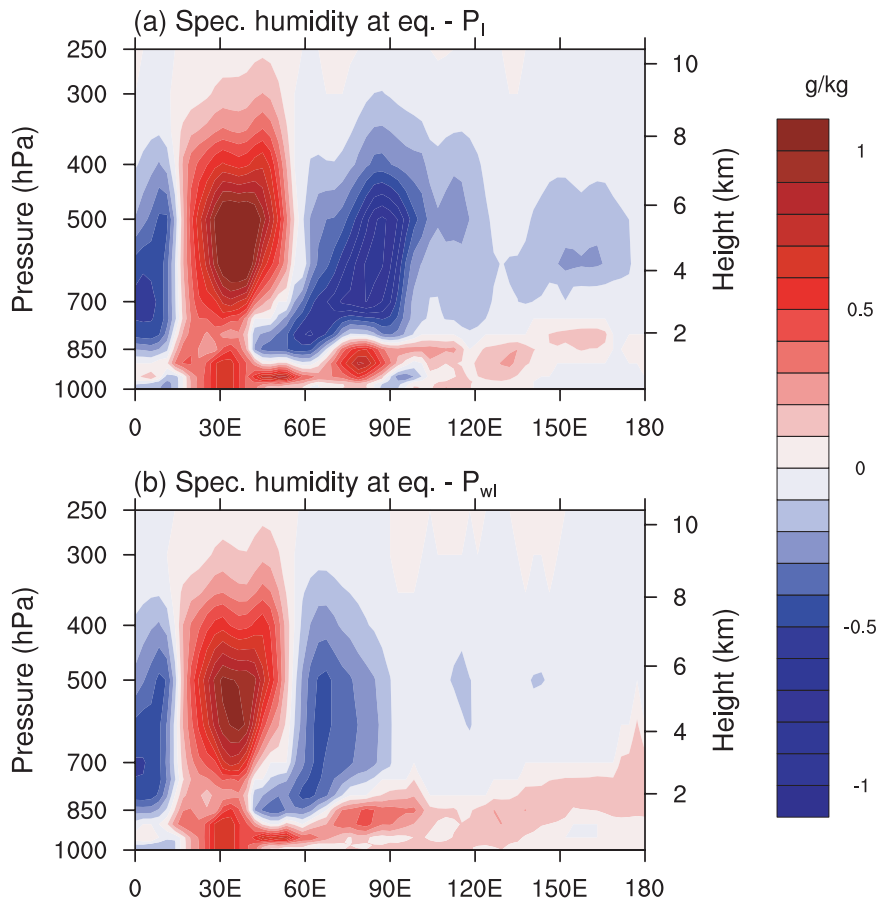
FIG. 10. Cross section of specific humidity anomalies centered at the equator for (a) P_I and (b) P_{wI}, averaged over the October–November months (g kg^{-1}). Colors indicate significant anomalies at the 90% CL as estimated by a two-tailed t test.

May and the October–November months (Fig. 3b in Hastenrath 2007). In the P_I case, the U_{EQ} anomaly relative to the CNTRL becomes increasingly negative after February. Strengthening of the easterly anomalies in the surface wind is especially rapid from August to October, reaching easterly wind anomalies in excess of 2.5 m s^{-1}. These U_{EQ} anomalies are of comparable magnitude to the U_{EQ} seasonal mean of 3 m s^{-1} in Hastenrath (2007) and thus represent a considerable weakening (or even a reversal, in some instances) of the overall westerly flow.

In observations, Black et al. (2003) find extreme IOD events associated with a weakening of the predominant westerly flow, a reduction of moisture transport away from East Africa, and thus enhanced short rains. Similarly for Tanzania, Mapande and Reason (2005a,b) indicate that easterly flow anomalies slow eastward propagation of intraseasonal anomalies and thus allow rain-inducing convection to remain over Tanzania for longer periods of time. In our experiments, the P_{eI+wI} case also shows strengthened easterly anomalies in the

second part of the year, though of lower magnitude than those seen in P_I. Only moderate easterly anomalies develop for the P_{wI} and P_{eI} cases. As previously demonstrated, the easterly anomalies in surface wind are closely linked to enhanced East African rainfall (Fig. 7; see also Goddard and Graham 1999; Black et al. 2003; Mapande and Reason 2005a; Hastenrath 2007). The development and magnitude of U_{EQ} in the different experiments presented here could thus provide an indication of the importance of the individual (and combined) SST anomaly poles.

6. Summary and conclusions

We have investigated the effect of a characteristic Indian Ocean SST pattern, with signatures of both the IOD and SIOD, on equatorial East African rainfall during the October–November season in AGCM ensemble experiments. In observations, enhanced East African precipitation is associated with Indian Ocean SST anomalies closely resembling a tropical IOD event
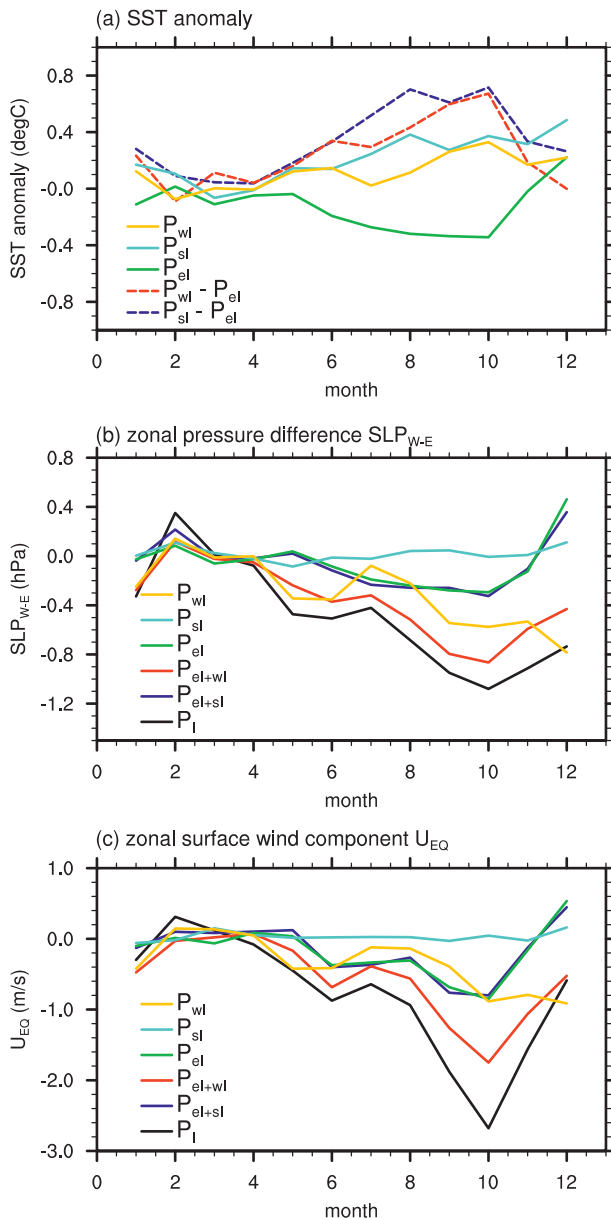
FIG. 11. (a) Seasonal cycle of SST anomalies (°C) spatially averaged over the poles used in the perturbation experiments (solid lines) and for the difference in SST anomalies for $P_{wI} - P_{eI}$ and $P_{sI} - P_{eI}$ (dashed lines). Seasonal cycle of the anomaly of the perturbation experiments relative to the CNTRL for (b) zonal SLP difference SLP_{W-E} (hPa) for 7°N–7°S, 39°–51°E − 7°N–7°S, 90°–101°E and (c) zonal surface wind component U_{EQ} (m s^{-1}) averaged over 4°N–4°S, 59°–90°E.

(Fig. 3; see also Black et al. 2003; Clark et al. 2003). The SST anomaly pattern used in the AGCM simulations in this study is very similar to that obtained when compositing SST for years with extreme wet conditions during the short rain season over East Africa. In addition to employing SST anomalies over the entire Indian

Ocean, we also assessed the contributions of individual (and combined) poles of the IOD and SIOD to above-average precipitation over East Africa.

Enhanced short rains in East Africa are driven predominantly by the local warm SST anomalies in the western Indian Ocean, while the eastern cold pole is of lesser importance (Figs. 4 and 5). The SST anomalies result in locally reduced SLP anomalies centered over the western Indian Ocean warm pole and the East African coast, and also extending west to the south of Africa. The SLP anomalies induce strengthened westerly airflow over central Africa and easterly onshore anomalies from the Indian Ocean that merge over the coast of equatorial East Africa. Thus, a strong anomalous convergence of moisture flux anomalies occurs over much of equatorial East Africa, with weaker divergent anomalies evident in central equatorial Africa. The warm SST anomalies in the western Indian Ocean result in increased latent heat flux, atmospheric moisture content due to local evaporation, and enhanced local convective activity. The pattern of large-scale circulation changes over the tropical Indian Ocean and adjacent landmasses is consistent with an anomalous strengthening of the Walker cell. Previous work linked enhanced East African rainfall and changed zonal flow anomalies to the zonal SST and zonal pressure gradient across the equatorial Indian Ocean associated with an IOD event (e.g., Saji et al. 1999; Webster et al. 1999; Black et al. 2003). However, we demonstrate that the wind, and thus moisture, convergence over equatorial East Africa is a predominantly local response forced by the warm SST anomalies in the western tropical Indian Ocean. Despite the importance of the western pole shown here in AGCM simulations, observations suggest that the western warm pole generally occurs in concert with a cold eastern pole. Therefore, the importance placed on the zonal gradient in SST, pressure, and winds in previous observational studies seems justified.

The seasonal development of characteristic indices of the zonal circulation in the equatorial Indian Ocean for the different experiments further confirms the importance of the western Indian Ocean warm pole in modulating East African rainfall. The SST anomalies associated with the various poles and the zonal gradient across the Indian Ocean intensify over the course of the year to peak during the October–November season. Similarly, the zonal circulation anomalies, in response to the gradually intensifying SST anomalies and to the seasonal cycle in the Indian Ocean Walker circulation, reach maximum values at the time of the East African short rains. The results suggest that the development of the anomalies in the zonal pressure gradient and especially the surface wind component is very rapid over the two months prior

to the short rain season in East Africa. This has implications for the usefulness of these indices as predictors in seasonal forecasting of East African rainfall. Hastenrath et al. (2004) find that the sudden development of the zonal circulation cell and the lack of long-lived precursors seriously hamper its usefulness as predictors for East African rainfall. The results of the present study regarding the importance of the local western SST pole suggest that future work into predictors for western Indian Ocean SST anomalies might benefit seasonal forecasting of East African rainfall. Implementing the Indian Ocean observing system in the western Indian Ocean should therefore be a high priority. At present, moored arrays are only partially in place, with most gaps being in the west (additional information is available online at http://www.clivar.org).

Examining a suite of model simulations with enhanced greenhouse gas forcing for the twenty-first century, as part of the Intergovernmental Panel of Climate Change Third Assessment Report, Hulme et al. (2001) find decreases in East African JJA rainfall, with the amount of change highly dependent on the emission scenarios used. Conversely, increased rainfall is projected for the December–February season (Hulme et al. 2001). Furthermore, de Wit and Stankiewicz (2006) assess the impact of future projected changes in precipitation patterns on surface water availability and drainage across Africa, finding that even small changes in rainfall can have considerable impacts on water availability because of the nonlinear relationship of rainfall and surface drainage. While drought-stricken areas of southern Africa are unlikely to experience improved conditions, East Africa might expect increases in surface water availability because of small projected increases in precipitation, translating into a shift from the unstable to the wet regime (de Wit and Stankiewicz 2006). The present study provides additional insight into the connection between slowly varying SST patterns and the modulation of East African precipitation. As such, it points toward the possibility of improved seasonal forecasting—a vital component in managing water resources in light of projected climate change.

REFERENCES

Behera, S. K., and T. Yamagata, 2001: Subtropical SST dipole events in the southern Indian Ocean. *Geophys. Res. Lett.,* **28,** 327–330.

——, R. Krishnan, and T. Yamagata, 1999: Unusual ocean-atmosphere conditions in the tropical Indian Ocean during 1994. *Geophys. Res. Lett.,* **26,** 3001–3004.

Birkett, C., R. Murtugudde, and R. Allan, 1999: Indian Ocean climate event brings floods to East Africa's lakes and the Sudd Marsh. *Geophys. Res. Lett.,* **26,** 1031–1034.

Black, E., J. Slingo, and K. R. Sperber, 2003: An observational study of the relationship between excessively strong short rains in coastal East Africa and Indian Ocean SST. *Mon. Wea. Rev.,* **131,** 74–94.

Bowden, J. H., and F. H. M. Semazzi, 2007: Empirical analysis of intraseasonal climate variability over the Greater Horn of Africa. *J. Climate,* **20,** 5715–5731.

Broad, K., and S. Agrawala, 2000: The Ethiopia food crisis—Uses and limits of climate forecasts. *Science,* **289,** 1693–1694.

Clark, C. O., P. J. Webster, and J. E. Cole, 2003: Interdecadal variability of the relationship between the Indian Ocean zonal mode and East African coastal rainfall anomalies. *J. Climate,* **16,** 548–554.

Colberg, F., C. J. C. Reason, and K. Rodgers, 2004: South Atlantic response to El Niño–Southern Oscillation induced climate variability in an ocean general circulation model. *J. Geophys. Res.,* **109,** C12015, doi:10.1029/2004JC002301.

Collins, W. D., and Coauthors, 2006: The Community Climate System Model version 3 (CCSM3). *J. Climate,* **19,** 2122–2143.

Deser, C., A. Capotondi, R. Saravanan, and A. S. Phillips, 2006: Tropical Pacific and Atlantic climate variability in CCSM3. *J. Climate,* **19,** 2451–2481.

de Wit, M., and J. Stankiewicz, 2006: Changes in surface water supply across Africa with predicted climate change. *Science,* **311,** 1917–1921.

England, M. H., C. C. Ummenhofer, and A. Santoso, 2006: Interannual rainfall extremes over southwest Western Australia linked to Indian Ocean climate variability. *J. Climate,* **19,** 1948–1969.

Epstein, P. R., 1999: Climate and health. *Science,* **285,** 347–348.

Feng, M., and G. Meyers, 2003: Interannual variability in the tropical Indian Ocean: A two-year time-scale of Indian Ocean Dipole. *Deep-Sea Res. II,* **50,** 2263–2284.

Fuchs, T., U. Schneider, and B. Rudolf, 2007: Global precipitation analysis products of the GPCC. Tech. Rep., Global Precipitation Climatology Centre, Deutscher Wetterdienst, Offenbach, Germany, 10 pp.

Funk, C., and Coauthors, 2005: Recent drought tendencies in Ethiopia and equatorial-subtropical eastern Africa. Tech. Rep., Famine Early Warning System Network at UCBS Climate Hazard Group, USGS National Center for EROS, and Chemonics International, 12 pp.

Giannini, A., R. Saravanan, and P. Chang, 2003: Oceanic forcing of Sahel rainfall on interannual to interdecadal time scales. *Science,* **302,** 1027–1030.

Gill, A. E., 1982: *Atmosphere–Ocean Dynamics.* Academic Press, 662 pp.

Goddard, L., and N. E. Graham, 1999: Importance of the Indian Ocean for simulating rainfall anomalies over eastern and southern Africa. *J. Geophys. Res.,* **104** (D16), 19 099–19 116.

Hack, J. J., J. M. Caron, S. M. Yeager, K. W. Oleson, M. M. Holland, J. E. Truesdale, and P. J. Rasch, 2006: Simulation of the global hydrological cycle in the CCSM Community Atmosphere Model version 3 (CAM3): Mean features. *J. Climate,* **19,** 2199–2221.

Hastenrath, S., 2007: Circulation mechanisms of climate anomalies in East Africa and the equatorial Indian Ocean. *Dyn. Atmos. Oceans,* **43,** 25–35.

——, A. Nicklis, and L. Greischar, 1993: Atmospheric-hydrospheric mechanisms of climate anomalies in the western equatorial Indian Ocean. *J. Geophys. Res.,* **98** (C11), 20 219–20 235.

——, D. Polzin, and P. Camberlin, 2004: Exploring the predictability of the 'short rains' at the coast of East Africa. *Int. J. Climatol.,* **24,** 1333–1343.

——, ——, and C. Mutai, 2007: Diagnosing the 2005 drought in equatorial East Africa. *J. Climate,* **20,** 4628–4637.

Hulme, M., R. Doherty, T. Ngara, M. New, and D. Lister, 2001: African climate change: 1900–2100. *Climate Res.,* **17,** 145–168.

Hurrell, J. W., J. J. Hack, A. S. Phillips, J. Caron, and J. Yin, 2006: The dynamical simulation of the Community Atmosphere Model version 3 (CAM3). *J. Climate,* **19,** 2162–2183.

Janowiak, J. E., 1988: An investigation of interannual rainfall variability in Africa. *J. Climate,* **1,** 240–255.

——, and P. Xie, 1999: CAMS–OPI: A global satellite–rain gauge merged product for real-time precipitation monitoring applications. *J. Climate,* **12,** 3335–3342.

Kalnay, E., and Coauthors, 1996: The NCEP/NCAR 40-Year Reanalysis Project. *Bull. Amer. Meteor. Soc.,* **77,** 437–471.

Kijazi, A. L., and C. J. C. Reason, 2005: Relationships between intraseasonal rainfall variability of coastal Tanzania and ENSO. *Theor. Appl. Climatol.,* **82,** 153–176.

Kistler, R., and Coauthors, 2001: The NCEP–NCAR 50-Year Reanalysis: Monthly means CD-ROM and documentation. *Bull. Amer. Meteor. Soc.,* **82,** 247–267.

Landman, W. A., and S. J. Mason, 1999: Changes in the association between Indian Ocean sea-surface temperatures and summer rainfall over South Africa and Namibia. *Int. J. Climatol.,* **19,** 1477–1492.

Latif, M., D. Dommenget, M. Dima, and A. Grötzner, 1999: The role of Indian Ocean sea surface temperature in forcing East African rainfall anomalies during December–January 1997/98. *J. Climate,* **12,** 3497–3504.

Li, T., B. Wang, C.-P. Chang, and Y. Zhang, 2003: A theory for the Indian Ocean dipole–zonal mode. *J. Atmos. Sci.,* **60,** 2119–2135.

Linthicum, K. J., A. Anyamba, C. J. Tucker, P. W. Kelley, M. F. Myers, and C. J. Peters, 1999: Climate and satellite indicators to forecast Rift Valley fever epidemics in Kenya. *Science,* **285,** 397–400.

Lyon, B., and S. J. Mason, 2007: The 1997–1998 summer rainfall season in southern Africa. Part I: Observations. *J. Climate,* **20,** 5134–5148.

Mapande, A. T., and C. J. C. Reason, 2005a: Interannual rainfall variability over western Tanzania. *Int. J. Climatol.,* **25,** 1355–1368.

——, and ——, 2005b: Links between rainfall variability on intraseasonal and interannual scales over western Tanzania and regional circulation and SST patterns. *Meteor. Atmos. Phys.,* **89,** 215–234.

Meehl, G. A., and J. M. Arblaster, 1998: The Asian–Australian monsoon and El Niño–Southern Oscillation in the NCAR Climate System Model. *J. Climate,* **11,** 1356–1385.

——, ——, and J. Loschnigg, 2003: Coupled ocean–atmosphere dynamical processes in the tropical Indian and Pacific Oceans and the TBO. *J. Climate,* **16,** 2138–2158.

——, ——, D. M. Lawrence, A. Seth, E. K. Schneider, B. P. Kirtman, and D. Min, 2006: Monsoon regimes in the CCSM3. *J. Climate,* **19,** 2482–2495.

Meyers, G., 1996: Variation of Indonesian Throughflow and the El Niño–Southern Oscillation. *J. Geophys. Res.,* **101,** 12 255–12 263.

——, P. McIntosh, L. Pigot, and M. Pook, 2007: The years of El Niño, La Niña, and interactions with the tropical Indian Ocean. *J. Climate,* **20,** 2872–2880.

Mutai, C. C., M. N. Ward, and W. Colman, 1998: Towards the prediction of East Africa short rains based on sea surface temperature-atmosphere coupling. *Int. J. Climatol.,* **18,** 975–997.

Nicholls, N., 1989: Sea surface temperatures and Australian winter rainfall. *J. Climate,* **2,** 965–973.

Ogallo, L. J., 1988: Relationships between seasonal rainfall in East Africa and the Southern Oscillation. *J. Climatol.,* **8,** 31–43.

Rayner, N. A., D. E. Parker, E. B. Horton, C. K. Folland, L. V. Alexander, and D. P. Rowell, 2003: Global analyses of SST, sea ice and night marine air temperature since the late nineteenth century. *J. Geophys. Res.,* **108,** 4407, doi:10.1029/2002JD002670.

Reason, C. J. C., 2002: Sensitivity of the southern African circulation to dipole sea-surface temperature patterns in the South Indian Ocean. *Int. J. Climatol.,* **22,** 377–393.

——, and D. Jagadheesha, 2005: A model investigation of recent ENSO impacts over southern Africa. *Meteor. Atmos. Phys.,* **89,** 181–205.

——, and M. Rouault, 2005: Links between the Antarctic Oscillation and winter rainfall over western South Africa. *Geophys. Res. Lett.,* **32,** L07705, doi:10.1029/2005GL022419.

——, R. J. Allan, J. A. Lindesay, and T. J. Ansell, 2000: ENSO and climatic signals across the Indian Ocean basin in the global context: Part I. Interannual composite patterns. *Int. J. Climatol.,* **20,** 1285–1327.

Rocha, A., and I. Simmonds, 1997a: Interannual variability of south–eastern African summer rainfall. Part I: Relationships with air-sea interaction processes. *Int. J. Climatol.,* **17,** 235–265.

——, and ——, 1997b: Interannual variability of southeastern African summer rainfall. Part II: Modelling the impact of sea-surface temperatures on rainfall and circulation. *Int. J. Climatol.,* **17,** 267–290.

Saji, N. H., B. N. Goswami, P. N. Vinayachandran, and T. Yamagata, A dipole mode in the tropical Indian Ocean. *Nature,* **401,** 360–363.

Santoso, A., 2005: Evolution of climate anomalies and variability of Southern Ocean water masses on interannual to centennial timescales. Ph.D. thesis, University of New South Wales, Sydney, Australia, 326 pp.

Smith, T. M., and R. W. Reynolds, 2003: Extended reconstruction of global sea surface temperatures based on COADS data (1854–1997). *J. Climate,* **16,** 1495–1510.

——, and ——, 2004: Improved extended reconstruction of SST (1854–1997). *J. Climate,* **17,** 2466–2477.

Ummenhofer, C. C., A. Sen Gupta, M. J. Pook, and M. H. England, 2008: Anomalous rainfall over southwest Western Australia

forced by Indian Ocean sea surface temperatures. *J. Climate,* **21,** 5113–5134.

Verdin, J., C. Funk, G. Senay, and R. Choularton, 2005: Climate science and famine early warning. *Philos. Trans. Roy. Soc. London,* **360B,** 2155–2168.

Verschuren, D., K. R. Laird, and B. F. Cumming, 2000: Rainfall and drought in equatorial east Africa during the past 1,100 years. *Nature,* **403,** 410–414.

von Storch, H., and F. W. Zwiers, 1999: *Statistical Analysis in Climate Research.* Cambridge University Press, 484 pp.

Webster, P. J., A. M. Moore, J. P. Loschnigg, and R. R. Leben, 1999: Coupled ocean–atmosphere dynamics in the Indian Ocean during 1997–98. *Nature,* **401,** 356–360.

Wijffels, S., and G. Meyers, 2004: An intersection of oceanic waveguides—Variability in the Indonesian Throughflow region. *J. Phys. Oceanogr.,* **34,** 1232–1253.

Xie, P., and P. A. Arkin, 1996: Analyses of global monthly precipitation using gauge observations, satellite estimates, and numerical model predictions. *J. Climate,* **9,** 840–858.

Zelle, H., G. J. van Oldenborgh, G. Burgers, and H. Dijkstra, 2005: El Niño and greenhouse warming: Results from ensemble simulations with the NCAR CCSM. *J. Climate,* **18,** 4669–4683.

Zhang, G. J., and H. Wang, 2006: Toward mitigating the double ITCZ problem in NCAR CCSM3. *Geophys. Res. Lett.,* **33,** L06709, doi:10.1029/2005GL025229.